Journal of Applied Fluid Mechanics, Vol. 18, No. 10, pp. 2504-2517, 2025.
Available online at www.jafmonline.net, ISSN 1735-3572, EISSN 1735-3645.
https://doi.org/10.47176/jafm.18.10.3458

Numerical Investigation and Performance Evaluation of Boiling Slug Flow Regime of Water Vapor in Vertical Tubes

F. Sharifi[1], M. Hassani[2] and R. Kouhikamali[3†]

[1] *Faculty of Mechanical Engineering, University of Guilan, Rasht, Iran*
[2] *Independent Researcher, Iran*
[3] *Department of Mechanical Engineering, Isfahan University of Technology, Isfahan, Iran*

†*Corresponding Author Email: r.kouhikamali@iut.ac.ir*

ABSTRACT

The boiling phenomenon and two-phase flow regimes have provoked extensive research due to the increased heat transfer coefficient and significant industrial applications. In order to model correct heat transfer of boiling, it is important to simulate its nucleation sites. In this work, boiling phenomenon simulation is carried out numerically in a vertical tube. The operating fluid is water which enters the tube with upward flow at saturated condition. Numerical investigation is carried out by Eulerian-Eulerian volume of fluid model in two-dimensional coordinate system. Slug flow simulation has been conducted by numerically simulating the embryonic bubbly flow at the beginning part of the tube and slugs have been created after formation of nucleation sites. To do so, heat and mass transfer during the flow motion is considered by the rate of mass and energy exchange between the phases and is added to governing equations. One of the key outputs of the numerical simulation is accomplishment of boiling slug flow pattern. Correspondingly, hydrodynamic and heat transfer characteristics of boiling flow regime like bubble detachment location, slug shape and size, local and average heat transfer coefficient are investigated. Furthermore, the effects of Reynolds and Boiling numbers have been studied. Reynolds number in the range of 27000 to 101000 has been considered. It is found that by doubling the Reynolds number, a 36% increase in mean heat transfer coefficient is observed. Additionally increase in the Boiling number by 60%, leads to 3% increase in the mean heat transfer coefficient.

Article History

Received February 18, 2025
Revised May 9, 2025
Accepted May 20, 2025
Available online August 5, 2025

Keywords:

Slug flow
Boiling
Numerical simulation
Flow pattern
Steam
Vertical tube

1. INTRODUCTION

Two-phase flows play an important role in industrial applications. Especially boiling and slug flow regimes have usages in industries such as geothermal power, chemical processes, petroleum industries of oil and gas, steam generators, kettle reboilers, production and transformation of hydrocarbons. Particular characteristics of boiling heat transfer and its wide use have attracted researches to experimental and numerical modeling. Accordingly, investigation of bubbly and slug flow regimes, as the main sections of boiling, can help contribute to design equipment such as boilers, evaporators and nuclear reactors.

Firstly, many experimental studies were carried out with the mainspring of generating an accurate correlation for in-tube boiling heat transfer coefficient (Chen, 1966; Shah, 1976; Gungor & Winterton, 1986; Steiner & Taborek, 1992). Available correlations were obtained by large extensive experimental data. Classifications of the correlations are dependent on the combination of nucleate and convective mechanism of the flow. The assumptions of superposition of mechanisms, graphical chart of heat transfer coefficient and power law type of boiling model were proposed. Following the experimental work, Sumith et al. (2003) studied characteristics of flow boiling heat transfer of water in a vertical tube under atmospheric pressure. The effects of mass flux, heat flux and quality on the boiling heat transfer coefficient in slug-annular or annular flow pattern were examined. Celata et al. (2011) experimentally studied flow patterns of two-phase flow of FC-72 in a single micro-tube. Heat transfer rates and evaluation of heat transfer correlations and models were demonstrated. Flow visualization of bubble and slug flow regimes were also investigated in an array of 13 thermally coupled rectangular micro-channels and the dominant effect of Weber number on the outlet flow were found out

NOMENCLATURE

Bo	boiling number	*S*	mass source term
C_f	mass transfer intensity	S_h	energy source term
Cp	specific heat at constant pressure	t	time
d	diameter	T	temperature
E	mass weighted average energy	V	velocity
F	force	α	volume fraction
g	gravitational acceleration	μ	dynamic viscosity
G	mass flux	ρ	density
h	heat transfer coefficient	σ	surface tension
h_{fg}	latent heat of evaporation	f	liquid
K	thermal conductivity	g	gas
P	pressure	q	the phase q
q"	heat flux	sat	saturation

(Lagus & Kulacki, 2012). Ling et al. (2021) observed the influence of microbubbles on the occurrence of slugs and the flow pressure fluctuation. Wang et al. (2021) observed slug flow pattern in a vertical air- water flow and investigated its hydrodynamic characteristics including pattern transition region, local void fraction, Taylor bubble gas velocity and length by a developed method based on machine learning. Etminan et al. (2022) collected correlations of liquid thickness of slug flow in addition to different studies of hydrodynamics and flow patterns in mini and micro channels with different cross-sectional area. Visualization of air-water slug flow in a rectangular cross-section micro channel was experimentally carried out by Shin et al. (2023). They also studied fluctuations of local pressure of the mixture flow in the channel for discussing morphology of slugs in different types of slug flows. Etminan et al. (2023) experimentally and numerically studied flow patterns, pressure drop, heat transfer and film thickness of water-oil Taylor flow in a mini-channel and studied the influences of channel diameter, oil viscosity and flow rate.

In recent years with propagation in utility of fluid dynamics codes, numerical simulation of two-phase flows has developed widely. Among these models, the wall heat flux partitioning model can predict mean vapor volume fraction and wall temperature distribution with good agreement with experiments. By using this model in Ansys CFD software, Krepper et al. (2007) and Li et al. (2011) simulated subcooled boiling in the fuel assembly and boiling phenomenon in vertical channels, respectively. Krepper and Rzhak (2011) investigated the capabilities of CFD wall boiling model with R12 as the working fluid and discovered the effects of some thermo-hydraulics parameters such as gas volume fraction, gas velocity, liquid temperature and bubble size from experimental results and simulated them with the numerical model. Mehdipour et al. (2016) studied heat transfer characteristics of bubbly boiling flow regime of water in cooling passages of internal combustion engines numerically by the mixture model. The effects of surface tension have been ignored in their study.

Besides prediction of mean values of boiling flow patterns, it is needed to involve some algorithms for reconstruction of the interface. Schepper et al. (2008) simulated gas/vapor-liquid two-phase co-current horizontal flow regimes with the volume of fluid (VOF) multiphase flow model, by using the piecewise linear interface calculation (PLIC) algorithms. A good agreement between the simulated and expected flow regime for water-air flow was obtained. Medina et al. (2015) used slug tracking method and added heat transfer to simulate slug flow of non-boiling gas-liquid. Detection of slug flow regime of air-water flow besides annular, wispy annular and churn flow pattern is also investigated by VOF method and PLIC algorithm (Hassani et al., 2020). Schmelter et al. (2020) simulated slug flow of liquid (oil and brine water) and gas (nitrogen) in large horizontal pipes. Jaeger et al. (2018) simulated slug flow of air and water and observed that VOF approach with the geometrical reconstruction scheme leads to a better agreement in comparison with the experimental data for simulation of compressible flow. Simões et al. (2014), by means of the finite volume method and slug capturing approach in a high-resolution mesh investigated non-boiling heat transfer of transition of stratified to slug flow regime of gas-liquid flow in a horizontal pipe. Yan and Che (2011) investigated the hydrodynamics of the slug flow and the mechanism of the slug flow inducing corrosion with and without dispersed small bubbles. Taha and Cui (2006) investigated the motion of the single Taylor air bubble numerically by the VOF method in the vertical tubes. The shape and velocity of the slugs and the velocity distribution were computed and agreed favorably with the published experimental findings. Etminan et al. (2021), based on CFD simulation, investigated gas-liquid and liquid-liquid slug flow in a microchannel with a sudden expansion for studying flow hydrodynamics. They (Etminan & Muzychka, 2024) also investigated the hydrodynamics and heat transfer characteristics of liquid-liquid Taylor flow by a novel numerical method. They studied the importance of phases viscosity differences on the slug frequency and discovered heat transfer enhancement of shorter liquid plug region.

In the boiling flow, subcooled or saturated liquid enters the tube. Under the effect of heat flux and flow parameters, the quality gradually increases and liquid changes to vapor. Accordingly, it requires to model the vapor generation and interface tracking simultaneously. Film boiling or condensation flow, due to the continuous separate interface, can be modeled more straightforwardly. Kouhikamali (2010) simulated condensation of vapor by considering the linear distribution of temperature profile of condensate near the wall of the cylindrical vertical channels in multiple effect

desalination systems and modeled the amount of mass transfer in condensation. Yang et al. (2008) simulated the slug flow of R141B in a horizontal coiled tube using VOF multiphase flow model. The numerical prediction of phase evolution was in good agreement with the experimental observations. The temperature profile and heat transfer were also investigated. Sun et al. (2012) developed the phase change model with the VOF method for the case in which both unsaturated and saturated phases are present. The accuracy of the new vapor–liquid phase change model is verified by two-dimensional film boiling problem. Magnini et al. (2013) simulated multiple sequential slugs in horizontal microchannel with the volume of fluid interface capturing method with external functions to better estimate surface tension and evaporation phase change. Pan et al. (2016) proposed a VOF-based flow boiling model with features that enable cost-effective simulation of two-phase flow and heat transfer in realistic geometries. In this model, phase change at the liquid–vapor interface is predicted by using a saturated-interface-volume phase change model which is validated against the analytical solution for a one-dimensional Stefan problem. Mehdizadeh Momen et al. (2016) developed an analytical model to calculate pressure drop of slug flow. Magnini and Thome (2016) used Tanasawa model for phase change and modeled saturated flow boiling of slug flow regime in micro-channels. They used the VOF model to track the interface and captured the slugs after generating the stream of bubbles with a constant frequency. Motenegro et al. (2016) investigated a CFD based approach in order to simulate slug flow. They compared the accuracy of results for different meshes to tradeoff between accuracy and computational cost. Ferrari et al. (2018) simulated boiling slug flow in square micro-channels by using VOF method and Tanasawa model for phase change in finite volume solver OpenFOAM. Hassani and Kouhikamali (2020) showed that Lee phase change model can accurately predict boiling and evaporation in falling film evaporation of R-245fa on horizontal tube.

Numerical modeling of boiling slug flow regime is accompanied with continuous change in phases interface. This issue is investigated in this manuscript. The elaborated understanding of slug flow regime requires full examination of nucleation boiling which lacks in previous studies. Therefore, numerical modeling of saturated water boiling flow regime in a vertical upward tube is simulated based on the VOF model. In order to simulate the slug flow regime, initiation of nucleation boiling flow of water and bubbly flow is also covered in the modeling. Suitable parameterization of numerical simulation of slug flow regime leading to problem convergence and favorable accuracy is found out as the main goal. Following that, hydrodynamic and heat transfer characteristics of slug flow regime is studied completely. In addition, the effects of Reynolds and Boiling numbers on the main parameters of the problem are determined.

2. NUMERICAL SIMULATION

2.1 General Aspects

In this article, numerical transient simulation of two-phase flow has been carried out by VOF model. This model is based on Eulerian-Eulerian approach of CFD multiphase modeling which treats two phases as continuum. In the VOF model, phase distribution is based on the concept of fractional volume of fluids. In order to define the flow state at each computational cell, volume fraction of each phase has been described and tracked throughout the domain. Based on the fluid volume fraction which moves through a fixed cell, the phase position can be identified.

$$\alpha_q = V_q/V \tag{1}$$

where α_q is the volume fraction of qth phase and V denotes volume. $\alpha_q = 1$ indicates that the cell is full of qth phase. $\alpha_q = 0$ represents that the cell is void of qth phase, and $0 < \alpha_q < 1$ declares that the cell includes liquid-vapor interface (Hirt & Nichols, 1981). In the problem of boiling process, Eq. (1) is used to solve the volume fraction of vapor phase while the liquid volume fraction is obtained from the fact that the cell is occupied by phases with the total volume fractions equal to unity.

$$\sum_{q=1}^{n} \alpha_q = 1 \tag{2}$$

2.2 Governing Equations

In the VOF model, capturing the phase volume fraction and recognition of interface position are accomplished by solving volume fraction continuity equations. One set of Navier-Stokes momentum and energy equations are solved for two phase flow and the resulting velocity, pressure and temperature fields are shared among the phases.

In multiphase flows with phase change, it is needed to consider mass transfer between phases and use it in mass conservation equations as the following form:

$$\partial \alpha_f/\partial t + \nabla.\left(\vec{V}\alpha_f\right) = -S/\rho_f \tag{3}$$

$$\partial \alpha_g/\partial t + \nabla.\left(\vec{V}\alpha_g\right) = S/\rho_g \tag{4}$$

In the above equations, subscripts f and g denote water and vapor, respectively. $\vec{V}$ is the velocity vector and ρ refers to density. S is defined as the source term of mass transfer. In this problem, S is modeled based on the physics of evaporation and condensation mechanism (Lee, 1979). The amount of evaporation or condensation depends on mass transfer rate of phase change and deviation of cell's temperature from saturated one. In the case of evaporation, if the cell temperature (T) is equal or greater than saturation temperature (T_{sat}), mass transfer from liquid to vapor and evaporation occurs. Equation (5) shows the mass transfer model proposed by Lee (1979).

$$T \geq T_{sat} \rightarrow S = C_f \alpha_f \rho_f \left(T - T_{sat}\right)/T_{sat} \tag{5}$$

In this equation, C_f stands for mass transfer intensity factor with unit s^{-1}. It is an empirical coefficient and can be interpreted as a time relaxation coefficient. Very large values of this parameter cause divergence and instability in numerical problems (Lee, 1979). It was noticed that by reducing time step and mesh size, in order to attain result independence from mesh and time step size, the dependence of C_f is eliminated (Hassani & Kouhikamali,

2020). In this case this coefficient is considered as constant and equal to 40 s^{-1}.

The momentum equation of the mixture phase can be expressed as follows.

$$\partial(\rho\vec{V})/\partial t + \nabla.(\rho\vec{V}\vec{V}) = -\nabla P + \nabla.\left(\mu\left(\nabla\vec{V} + \nabla\vec{V}^{T}\right)\right) + \rho\vec{g} + F_{\sigma} \quad (6)$$

where, P is pressure, $\vec{g}$ is gravitational acceleration vector and F_σ is the source term related to surface tension (σ) and is calculated via continuum surface force (CSF) of Brackbill et al. (1995). It can be expressed as the following form.

$$F_{\sigma} = \sigma(\nabla.n)\nabla\alpha \quad (7)$$

The energy equation with source term of energy transfer is in the following form.

$$\partial(\rho E)/\partial t + \nabla.\left(\vec{V}(\rho E + P)\right) = \nabla.(K\nabla T) + S_h \quad (8)$$

K denotes thermal conductivity and S_h consists interfacial heat transfer. It is obtained from mass transfer source term.

$$S_h = S.h_{fg} \quad (9)$$

where h_{fg} is the latent heat of evaporation at operating pressure. In the VOF model, energy is defined as mass weighted average as expressed as follows.

$$E = \frac{\alpha_f\rho_f E_f + \alpha_g\rho_g E_g}{\alpha_f\rho_f + \alpha_g\rho_g} = \frac{(1-\alpha)\rho_f E_f + \alpha\rho_g E_g}{(1-\alpha)\rho_f + \alpha\rho_g} \quad (10)$$

where E_f and E_g are based on the specific heat (C_p) of liquid and vapor phases and are expressed as below.

$$E_f = C_{Pf}(T - 298.15) \quad (11)$$

$$E_g = C_{Pg}(T - 298.15) \quad (12)$$

In order to simulate the turbulence of the problem, k-ε Realizable turbulence equations are solved for the flow (Shih et al., 1995) and the enhanced wall function formulation is used to simulate the near wall layer (viscous layer) correctly.

2.3 Discretization and Solution Method

Discretization of the transport equations is carried out by finite volume method. The Green-Gauss node-based method is used for evaluation of numerical gradients. The node-based in comparison with the cell-based method leads to decrease numerical errors. The second order upwind of discretization scheme is used for momentum, energy and the two turbulent equations. In order to capture the interface of liquid-vapor, the Geo Reconstruct discretization scheme is used for volume fraction equation. Geo Reconstruct scheme captures the liquid-vapor interface within each computational cell by using a piecewise linear approach. This scheme is the most accurate one and is applicable for general unstructured meshes. For interpolation of pressure equation, PRESTO! Scheme is utilized. Improvement of convergence rate for pressure-velocity coupling is performed by PISO algorithm. The pressure implicit with splitting of the operators is a part of the SIMPLE family of algorithms which is based on a higher degree of the approximate relaxation between the correlations for pressure and velocity. This algorithm performs two additional corrections; neighbor and skewness correction which improves the efficiency of the calculation.

The under relaxation factors for solving pressure, momentum, energy, density, body force, turbulent kinetic energy, turbulent dissipation rate and turbulent viscosity are considered 0.85, 0.15, 0.3, 0.5, 0.5, 0.2, 0.8, and 0.2 respectively.

The other important factor for accurate simulation of complex liquid-vapor interface is the choice of suitable time step. In the two-phase flows, the courant number and consequently time step size should be small enough to capture the phase change correctly without causing numerical divergence. In the current numerical simulation, adaptive time step is used in each time step; therefore, time step size is calculated from constant courant number. Exceeding the specified courant number leads to smaller time step size. The average time step size that is used in this simulation was $\Delta t = 10^{-5}$s.

The current problem has been solved by the commercial CFD code of Ansys Fluent 19.1.

3. GEOMETRICAL CONFIGURATION

3.1 Boundary Conditions

The state of the current study is the nucleation boiling of upward flow of water at saturated condition. The problem is simulated in the two-dimensional coordinate system. The tube diameter and the tube length are 12.7 mm and 1 m, respectively. According to Fig. 1, the wall is heated at constant flux in such a way that the flow is located in the slug region of Bennett et al. map (Bennett et al., 1965) and the no-slip condition is applied to the wall. The outlet pressure is taken constant. Single flow of water enters the tube at saturated pressure of 68 bar. Also, the computational domain is axisymmetric relative to the axis of the tube. Figure 1 shows the computational domain and boundary conditions of the problem.

3.2 Computational Mesh

The flow domain of the tube is discretized by a uniform computational mesh. The mesh includes square cells with a minimum deviation of the aspect ratio with the standard one. In order to obtain bubble formation accurately at the wall, the cells are refined by using boundary layer mesh. Also, due to slug capturing at the center of the tube, the computational mesh is fined enough at the center.

A mesh independence of numerical study is considered. Four cases with computational cell number of 320000, 480000, 640000 and 960000 are generated based on fining the first cell size and maintaining the ideal aspect ratio. The results of the study ensure that, in order to capture the water-vapor interface, the finer computational

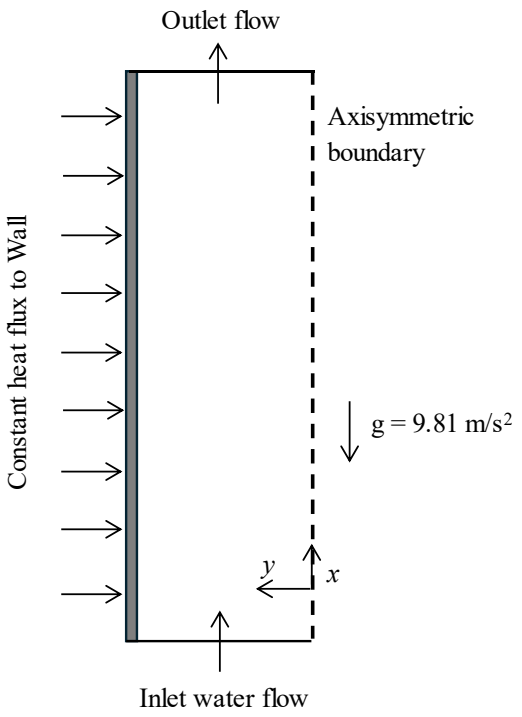

Fig. 1 Schematic of problem and boundary conditions

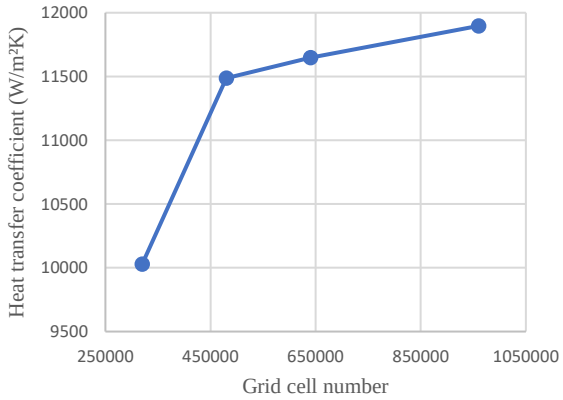

Fig. 2 Grid independence procedure for heat transfer coefficient

mesh leads to the more accurate interface tracking. Therefore, the desirable grid is the one with small changes in flow parameters and pattern after more fining. By fining the mesh, the value of mean heat transfer coefficient is changed 16%, 3% and 2% in comparison with the last grid. The change of heat transfer coefficient by mesh number is shown in Fig. 2. The flow pattern of the grids with 640000 and 960000 meshes did not show considerable changes as well, therefore, the grid with 640000 cells is selected as

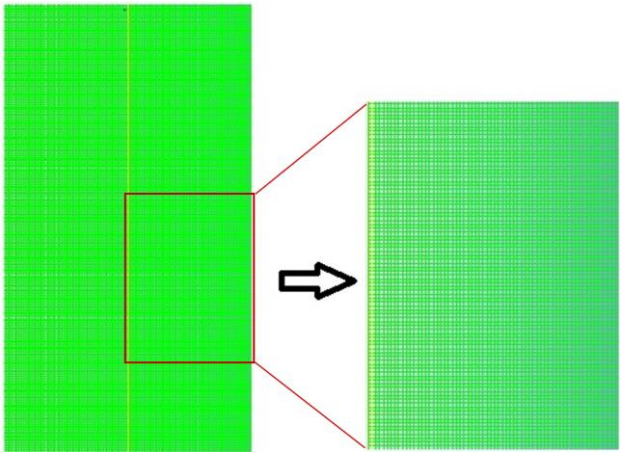

Fig. 3 Final generated grid for 23 mm of the tube

the final one. In the radial direction, the domain is divided to 64 elements and along the length of the tube 10000 divided cells are implemented. The size of the first cell in the region adjacent to the wall is $0.1 \times 0.1\ mm^2$. Final grid for a random part the tube with 23 mm length is indicated in Fig. 3.

4. VALIDATION OF THE CALCULATION

To investigate the validity of the numerical method, the CFD study has been authorized by an experimental case of flow boiling heat transfer of water (Sumith et al., 2003). The benchmark case is at the atmospheric pressure and temperature of 373.15 K and is performed in 100 mm long heated tube, with diameter of 1.45 mm. The mass flux of the inlet water is 44.1 kg/m^{2}s and the wall heat flux is 36 kW/m^2. Figure 4 displays the wall heat transfer coefficient of the CFD case along the tube length with the average heat transfer coefficient of 12760 W/m^2.K. The experimental heat transfer coefficient is approximately 13700 W/m^2.K. Quantitatively, the deviation of the CFD calculated heat transfer coefficient from the experimental case (Sumith et al., 2003) is about 6.9%.

Calculated numerical pressure drop and two-phase heat transfer coefficient of the flow are compared with Thome tables (Collier & Thome, 1994) and the Shah Correlation (Shah, 1982) for pressure drop and heat transfer coefficient, respectively. The case is at the pressure of 6.8 MPa and temperature of 557.02 K and is performed in a 1 m long heated tube, with diameter of 12.7 mm. The wall heat flux is 95110 W/m^2. Values of heat transfer coefficient and pressure drop are shown in Table 1. Deviation of the numerical value from experimental work of Shah for two-phase heat transfer differs about

Table 1 Comparison of numerical simulation with experimental correlations of Thome (Collier & Thome, 1994) and Shah (1982)

Parameter	Experimental correlation	Numerical simulation	Error
Mean heat transfer coefficient (W/m^2.K)	17050 (Shah, 1982)	11647.9	31%
Total pressure drop (Pa)	6004.4 (Collier & Thome, 1994)	5733.2	4.5%

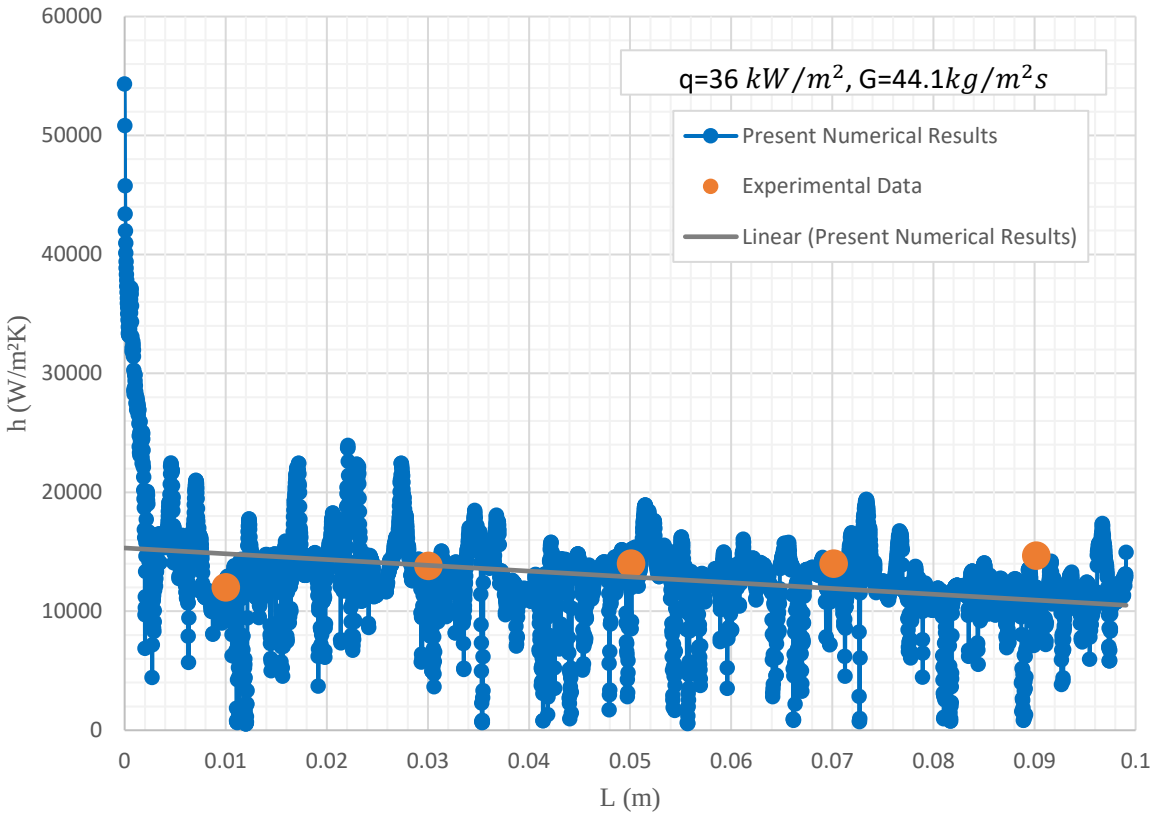

Fig. 4 Heat transfer coefficient variation along the tube in the present numerical simulation in comparison with the experimental data of Sumith (Sumith et al., 2003)

31%. This amount of error can be arised from some reasons. The major reason of the error is the complexity of the boiling flow regime variation and correspondingly simulation capabilities. The intricate interface phase change of boiling implicates in the generality of the Shah correlation for broad conditions of various fluids which is not compatible with the present condition completely.

5. RESULTS AND DISCUSSION

One of the interesting results of this work is to capture the slug flow regime along the tube. The flow pattern initiates at the beginning of the tube with bubbly flow and then in the middle, slug bubbles take place.

Figure 5 shows contours of vapor volume fraction along the tube with assortment of different parts of tube in detailed in (a) to (e) sections. Due to boiling, formation of initial bubble nucleates from the wall occurs. The increase in the water temperature above the saturation temperature fractionally causes boiling phenomenon to start. Gradually with increase in heat transfer from wall to the water, the vapor bubbles grow and finally detach from the wall to build up bubbly flow regime. Detachment of bubbles occurs because of the imbalance of forces acting on a vapor bubble. Buoyancy and hydrodynamic drag forces attempt to detach it, while surface tension and liquid inertia forces which result from displacement of liquid during bubble growth, act to prevent detachment. Bubble detaches from the wall when the drag forces acting on the bubble surmount the liquid inertia forces. Figure 5-b illustrates that approximately from about 25% of the second section of tube length (20-40 cm of the whole tube), balance of acting forces on the bubble conducts bubble detachment from heated wall and gently at about 30% of this section length, separation increases and bubbles are directed to the center of the tube.

The bubble size at the departure point is affected by the balance between the forces. Detached bubbles with higher velocity than liquid move toward the center of the tube against the gravity. Contours of vapor volume fraction at bubbly flow in Fig. 5-a and 5-b illustrate that the shapes of the bubbles in the bubbly flow regime at some sites are small spheres and at other sites, are slightly larger with spherical nose and a flat tail.

With increasing the bubble population and coalescence of small bubbles, slug flow regime starts to form at 40% of the tube length in section b. The contours of vapor volume fraction in the slug flow regime and variations and slug bubble growth up to the end of the tube are shown in Fig. 5-c, 5-d and 5-e.

The difference in the slug bubble size radially and longitudinally, is also observed in Fig. 5-c, 5-d and 5-e. Slug bubbles are shaped like prolate spheroidal. Gradually with increase of vapor quality in the flow, length of the slug bubbles extends significantly. Although it can change irregularly as can be seen at the end of the tube in Fig. 5-e. Formation of slugs includes a certain frequency of formation which changes continuously

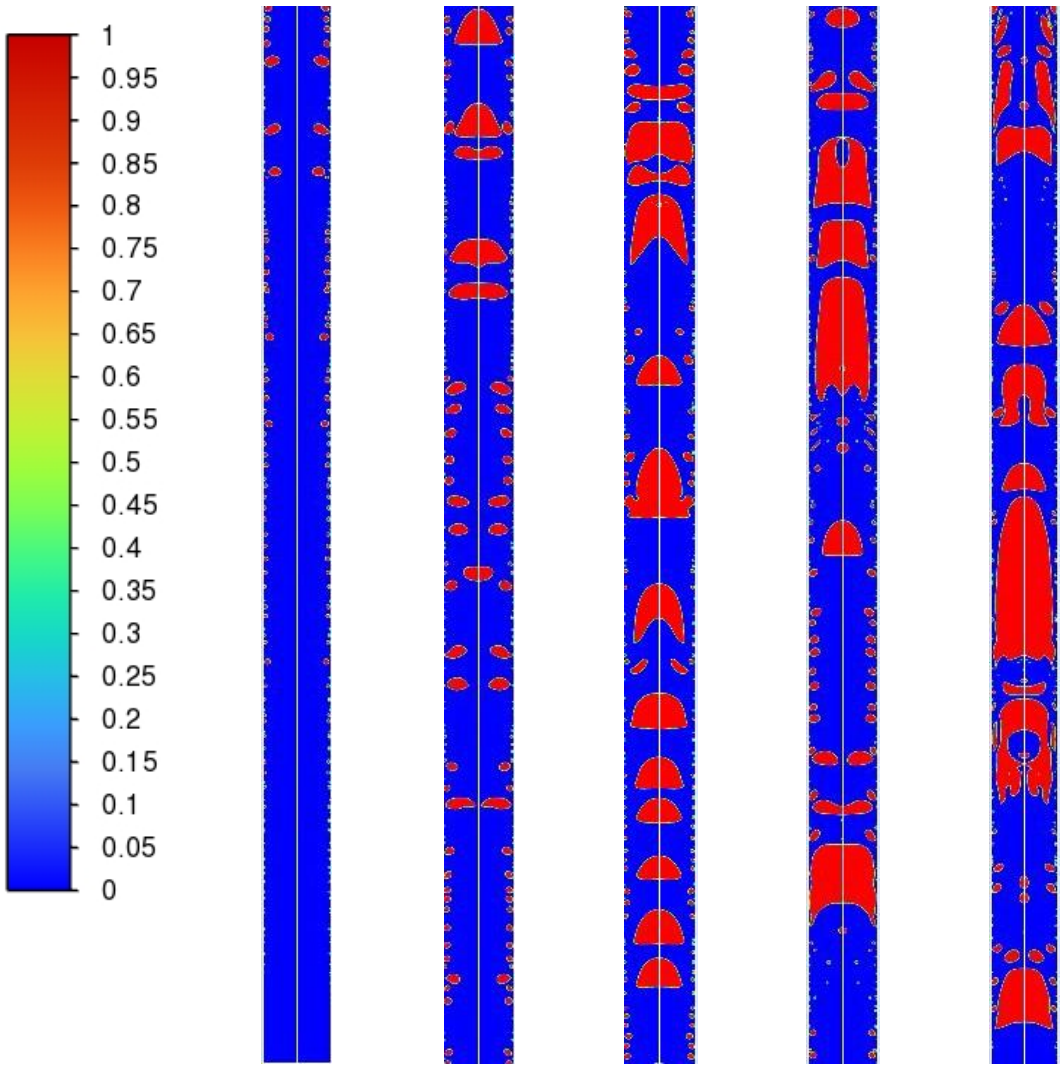

Fig. 5 Contours of vapor volume fraction of the bubbly and slug flow regime of water-vapor along different parts of tube: (a) 0-20 cm. (b) 20-40 cm. Slug flow regime: (c) 40-60 cm. (d) 60-80 cm. (e) 80 cm-1m

throughout the tube. One of the important features of the slug flow regime is liquid slugs; separated successive slug bubbles attaches to each other with liquid slugs. Figure 5-d and 5-e declare that liquid slug contains some small entrained vapor bubbles which are the resultant of slug bubbles' wake. Figure 5 also depicts that initial slugs at about 50% of the tube length are quietly small and well-ordered while the ones at the end of the tube are irregular and considerably elongated. High energy and velocity of terminal vapor slugs affect the liquid slugs at the tail of vapor slugs and cause them to extend in some parts.

Nature of the slug flow regime, due to the presence of vapor phase, necessitates high velocity and turbulence. Figure 6 shows the descriptive schematic of slug in nature, position of slug bubbles and velocity field vectors at a specified site of the tube. It shows that CFD slug flow pattern is compatible with the expected one in nature. It also declares that velocity vectors reach the maximum value of the flow at the slug bubble and not a notable radial velocity is seen along the tube. In addition, the liquid slug is affected remarkably by the velocity changes of vapor bubbles. Increase in the velocity of liquid slugs is quite considerable and differs from the velocity of water at the other sites of the tube. Furthermore, the intensity of turbulence due to high velocity of low-density vapor slugs increases and changes corresponding to the position of the slug bubbles.

One of the other investigations of the slug flow is the changes of the vapor slug shape at different heat flux values and accordingly outlet vapor quality. Figure 7 shows the variation of vapor and liquid slug shapes at the end and a certain range of tube length. Vapor outlet quantity of 2.5%, 4%, 5% and 6% corresponds to the heat flux of 47585, 76094, 95110, 114140 W/m^2 at Reynolds number of 54470. Reynolds number (Re), the ratio of inertial to viscous forces within the fluid is expressed as:

$$Re = \rho V d / \mu \tag{13}$$

Where d denotes tube diameter.

Because of higher values of heat flux applied to the wall, increase in the numbers of vapor slug at a constant

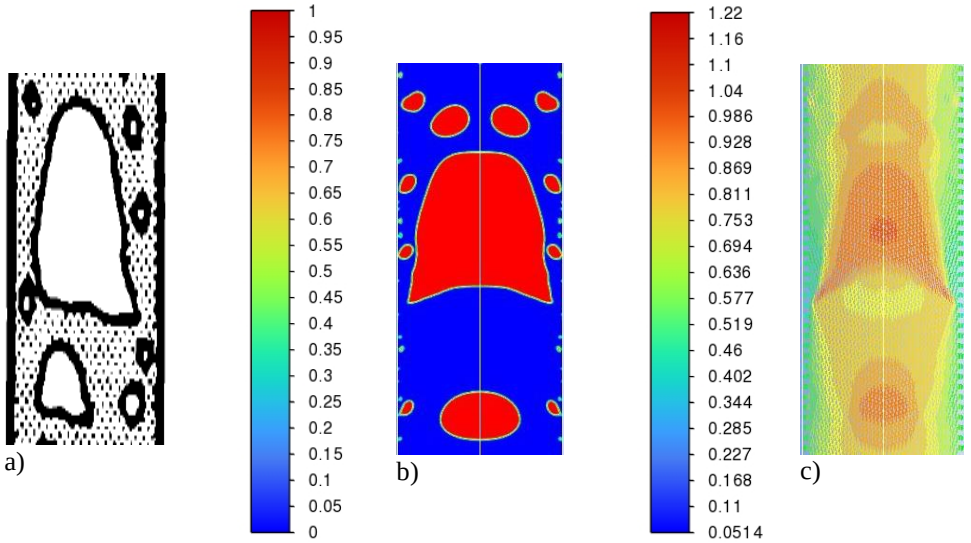

Fig. 6 (a) Descriptive schematic of slug in nature (Bennett, 1965), (b) Vapor volume fraction of slug bubbles, and (c) Velocity vectors (m/s) colored by magnitude at the location identified in part (b).

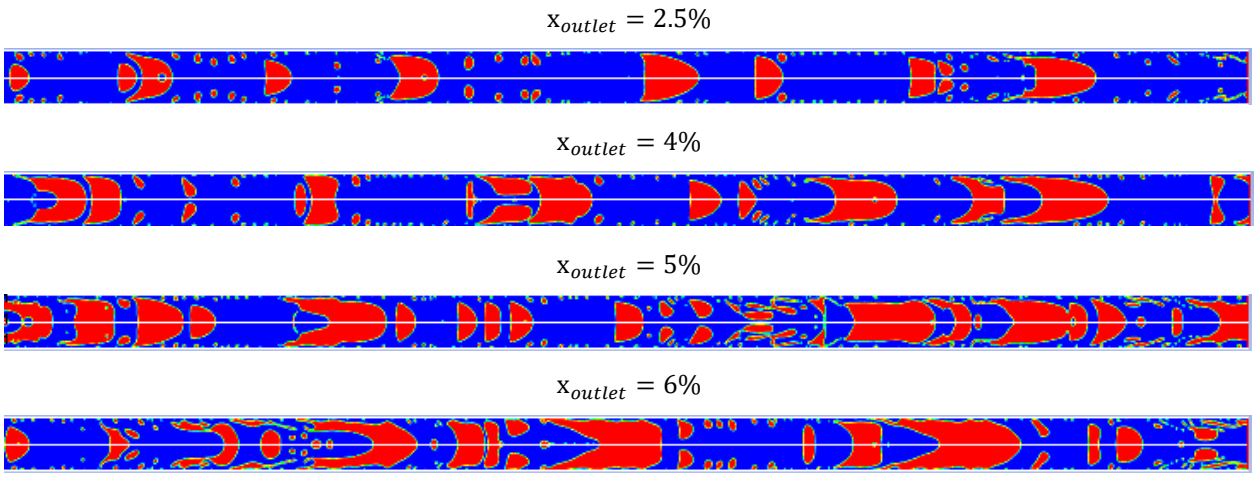

Fig. 7 Changes of slug size with different values of heat flux

range of x-coordinate is observed. Also, elongation of the leading slug bubbles extends noticeably. Increase of the vapor amount provokes the turbulence of the flow. Hence, the trailing vapor bubbles entrain in the liquid slug at the rear of vapor slugs and increase quantitatively and qualitatively. The other substantial point in the probe of the slug size is that the vapor slug diameter remains constant, as large as the order of tube diameter, and does not change significantly.

Figures 8 and 9 report the wall heat transfer coefficient and corresponding positions of bubbles or slugs by the vapor volume fraction individually. Heat transfer coefficient (h), the quantitative characteristic of heat transfer between the fluid and the surface is defined as follows:

$$h = q''/(T - T_{sat}) \tag{14}$$

where q'' is heat flux, T is temperature and *sat* denotes saturation.

The contribution of nucleation boiling and phase change mechanism is clear from the mean wall heat transfer coefficient. Some important points can be derived from the wall heat transfer distribution along the tube which are expressed as follows. Firstly, the heat transfer fluctuation is due to the nature of two-phase flow and presence of the different fluids throughout the tube. Secondly, the heat transfer fluctuation in the slug flow is slightly more than the bubbly flow regime, which is implied by Fig. 8 and 9. Due to the presence of vapor slugs beside bubbles near the wall, heat transfer coefficient includes more variations and changes than bubbly flow regime. In addition to release of latent heat in phase change phenomena in boiling regime, the relative high heat transfer coefficient in such flows is made based on some reasons. As shown in Fig. 8 and 9 and the corresponding nucleated bubbles and slugs and phase change from liquid to vapor, flow density near the wall decreases and velocity increases which is a main factor for a higher turbulence and enhancement of heat

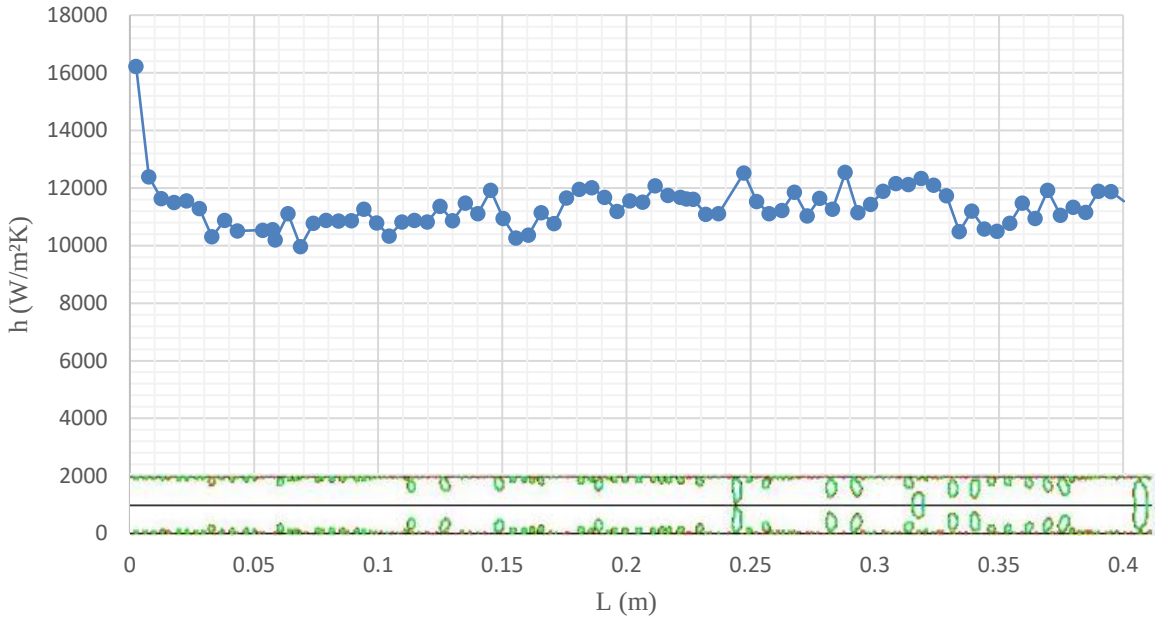

Fig. 8 Heat transfer coefficient distribution in the bubbly flow regime and corresponding volume fraction

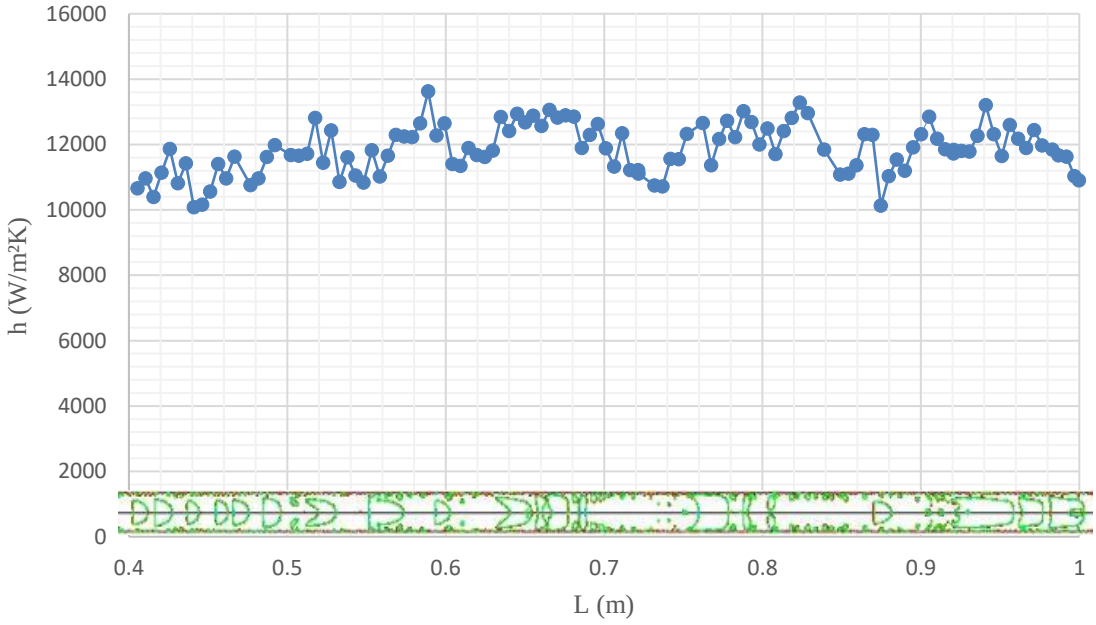

Fig. 9 Heat transfer coefficient distribution in the slug flow regime and corresponding volume fraction

transfer coefficient. Figure 10 shows velocity and turbulence intensity profiles of the flow in the slug flow regime. Figure 10 indicates higher velocity of flow in the vapor slugs due to the lower density. The velocity of water between slugs is also increased, providing from the vapor slug velocity and turbulence. Turbulence intensity increase near the wall and also phases interface is also indicated in this figure. In addition, bubble detachment from the wall breaks the boundary layer and causes a relatively uniform temperature in the tube. Heat transfer coefficient fluctuation clearly describes bubble detachment and formation near the wall.

Figure 11 shows the axial velocity variation along the tube at different inlet mass flow rates of water.

Applying heat flux on the wall besides saturation condition causes the boiling to occur. Axial velocity fluctuates due to the presence of two-phase flow which is the resultant of phase change. At lower inlet mass flow rate, axial velocity starts to fluctuate earlier than the others. It is observed that at a constant heat flux, the less mass flow rate enters, the more evaporation takes place. At lower mass flow rates, since the mass flow fraction is lower, the flow can obtain more energy to phase change. Therefore, vapor bubbles with specific properties approach the axial location earlier than cases with higher inlet mass flow rates.

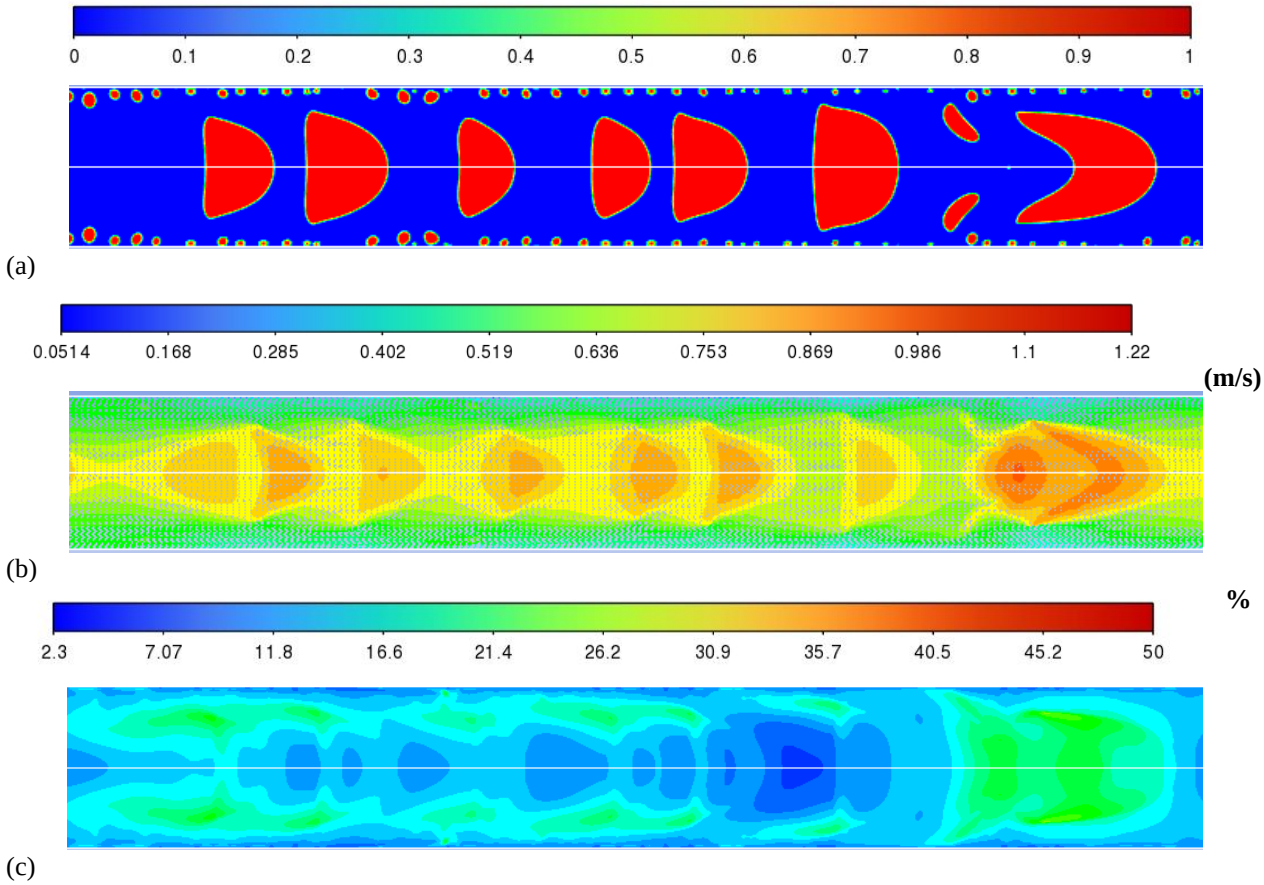

Fig. 10 Contour of (a) vapor volume fraction, (b) velocity and (c) turbulent intensity of slug flow regime

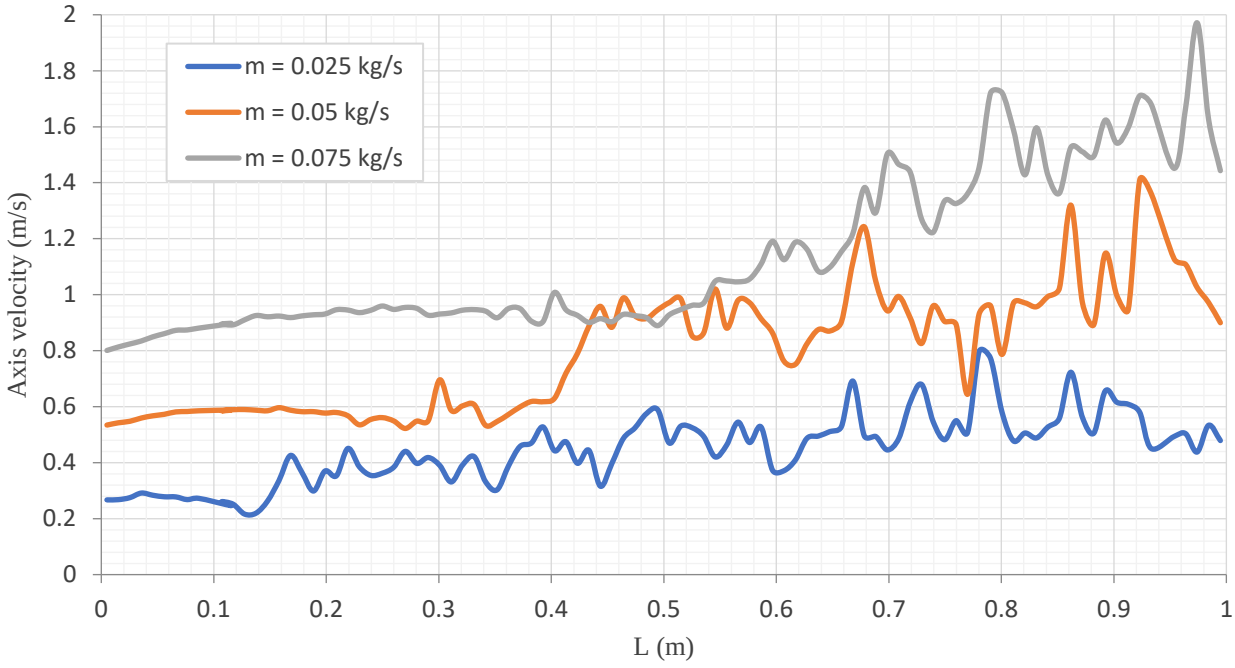

Fig. 11 axial velocity variation at different inlet mass flow rates of water

Heat transfer mechanism of water nucleation boiling is affected by many parameters such as mass flow rate, wall heat flux, geometrical configuration and physical properties of fluids. Based on these parameters, dimensionless groups of nucleation boiling are identified. In this study, two important dimensionless numbers, Reynolds and Boiling numbers, are discussed.

The effect of heat flux on the boiling is characterized by Boiling number. It indicates the ratio of the actual heat flux given to the flow relative to the maximum achievable heat flux by complete evaporation

Table 2 Effect of Reynolds number at a constant value of boiling number (Bo=1.58×10^{-4})

Case	Reynolds number	Inlet mass flow rate (kg/s)	Average location of bubble detachment (%)	Mean wall temperature (K)	Mean wall heat transfer coefficient (W/m^2.K)
1	27200	0.025	15	563.29	8005.36
2	40800	0.0375	25	565.13	9356.33
3	54400	0.05	30	566.31	10860.08
4	68000	0.0625	35	567.36	12339.16
5	817100	0.075	40	568.41	13668.9
6	108900	0.1	57.5	571.09	15596.91

Table 3 Effect of Boiling number at a constant value of Reynolds number (Re=54470)

Case	Boiling number	Wall heat flux (W/m^2)	Average location of bubble detachment (%)	Mean wall temperature (K)	Mean wall heat transfer coefficient (W/m^2.K)
1	9.52×10^{-5}	57070	34	562.75	10321.1
2	1.27×10^{-4}	76094	32.5	565.60	10621.67
3	1.58×10^{-4}	95110	30	566.31	10860.08
4	1.90×10^{-4}	114140	30	568.67	10942.05
5	2.20×10^{-4}	133164	26	570.13	11301.87

of the inlet liquid. It is defined as follows.

$$Bo = q''/Gh_{fg} \quad (15)$$

where q'' is heat flux and G denotes mass flux.

Table 2 points out the effect of inlet liquid Reynolds number on the output parameters of the problem. Inlet liquid Reynolds number is considered in the range of 27000 to 110000 and the boiling number remains constant at a value of 1.58×10^{-4}. In these conditions, the problem is preserved in the range of nucleation flow boiling despite the increase in the rate of phase change. Increase of inlet liquid Reynolds requires higher heat flux and inlet mass flow rate, which results in higher energy of the flow. Therefore, higher mean wall temperature and wall heat transfer coefficient are obtained. Quantitatively, by doubling the Reynolds number, a 36% increase in the mean heat transfer coefficient is observed.

Additionally, Table 2 shows the average bubble detachment of the bubbly flow at different Reynolds numbers. It infers that increasing the Reynolds number, defers the bubble detachment. In other terms in the nucleation boiling regime, increasing the Reynolds number prolongs initiation of slug flow regime and nucleation of bubbles from the wall is the dominant regime of the flow.

Boiling number is the other important dimensionless number which is of great significance. Table 3 shows the parametric studies of the flow on the boiling number. Five cases were investigated at a constant Reynolds number and inlet mass flow rate with the value of 54470 and 0.05 kg/s, respectively. It declares that by increasing the boiling number, heat flux and temperature of the wall increase. Therefore, the formation rate of vapor bubble on the wall promotes and accordingly outlet vapor quality at the range of slug flow increases. Also, it is inferred from Table 3 that higher boiling number due to increase of the amount of applied energy to each flow cell results in augmentation in phase change from liquid to vapor. Hence the average heat transfer coefficient increases as well.

The other parameter which is analyzed by boiling number is the detachment of the bubbles and average location of bubbly flow regime. It is shown in Table 3 that detachment of bubbles at higher boiling numbers occurs earlier at the tube. This happens due to increase in the given heat flux rather than ideal achievable heat flux of the total flow which is remained constant. Consequently, higher values of the boiling number at a constant Reynolds number lead to higher rate of evaporation. In other terms, a 60% increase in the Boiling number, leads to 3% increase in the mean heat transfer coefficient.

6. CONCLUSION

In this study, 2-D numerical simulation of boiling slug flow regime of water in vertical tubes is investigated. VOF multiphase method with suitable parameterization of numerical modeling of water-vapor slug flow regime leading to problem convergence and favorable accuracy is found out as the main goal.

The flow pattern of nucleation boiling regimes including bubbly and slug is detected correctly. The formation and variations of bubbles, liquid and vapor slugs have been observed. It is concluded that the higher values of wall heat flux and correspondingly outlet vapor quality led to more numbers of vapor slug with extension of slug elongation remarkably.

The effects of changing Re and Bo numbers have been studied on the flow pattern and main characteristics of hydrodynamics and heat transfer. Increasing Re number causes the bubble detachment to prolong and heat transfer to increase; by doubling the Reynolds number, a 36% increase in mean heat transfer coefficient was observed. In addition, boiling number increase causes slug bubble propagation, earlier bubble detachment and consequently heat transfer coefficient

augmentation in such a way that increase in the Boiling number by 60%, leads to 3% increase in the mean heat transfer coefficient.

ACKNOWLEDGEMENTS

The authors are grateful to high performance research center of Amirkabir University for parallel processing support.

CONFLICT OF INTEREST

The authors have no conflicts to disclose.

AUTHORS CONTRIBUTION

F. Sharifi: Conceptualization, Methodology, Software, Formal analysis, Writing – Original Draft. **M. Hassani:** Methodology, Formal analysis, Writing – Review & Editing. **R. Kouhikamali:** Supervision, Project administration.

REFERENCES

Bennett, A. W., Hewitt, A. W., Kearsey, H. A. (1965). Flow visualization studies of boiling at high pressure. *Proceedings of the Institution of Mechanical Engineers*. *180*(3C), 1-11. https://doi.org/10.1243/PIME_CONF_1965_180_119_02

Brackbill, J., Liou, W.W., Shabbir, A., Yang, Z., & Zhu, J. (1995). A new k-epsilon eddy viscosity model for high Reynolds number turbulent Flows - model development and validation. *Computers and Fluids*, *24*, 227–238.

Celata, G. P., Cumo, M., Dossevi, D., Jilisen, R. T. M., Saha, S. K., & Zummo, G. (2011). Visualisation of flow boiling heat transfer in a microtube. *Heat Mass Transfer*, *47*, 941–949. https://doi.org/10.1007/s00231-011-0846-0

Chen, J. C. (1966). Correlation for boiling heat transfers to saturated fluids in convective flow. *Industrial & Engineering Chemistry Process Design and development*, *5*, 322-329. https://doi.org/10.1021/i260019a023

Collier, G. J., & Thome, J. R. (1994). *Convective boiling and condensation.* Clarendon Press, Oxford.

De Schepper, S. C. K., Heynderickx, G. J., & Marin, G. B. (2008). CFD modeling of all gas–liquid and vapor–liquid flow regimes predicted by the Baker chart. *Chemical Engineering Journal*, *138*, 349–357. https://doi.org/10.1016/j.cej.2007.06.007

Etminan, A., & Muzychka, Y. S. (2024). Effects of flow characteristics on the heat transfer mechanism in Taylor flow. *International Journal of Heat and Mass Transfer*, *219*, 124917. https://doi.org/10.1016/j.ijheatmasstransfer.2023.124917

Etminan, A., Muzychka, Y. S., & Pope, K. (2021). Numerical investigation of gas-liquid and liquid-liquid Taylor flow through a circular microchannel with a sudden expansion. *The Canadian Journal of Chemical Engineering*, *100*(7), 1596-1612. https://doi.org/10.1002/cjce.24229

Etminan, A., Muzychka, Y. S., & Pope, K. (2022). Liquid film thickness of two-phase slug flows in capillary microchannels: a review paper. *The Canadian Journal of Chemical Engineering*, *100*(2), 325-348. https://doi.org/10.1002/cjce.24068

Etminan, A., Muzychka, Y. S., & Pope, K. (2023). Experimental and numerical analysis of heat transfer and flow phenomena in Taylor flow through a straight mini-channel. *Journal of Heat and Mass Transfer*, *145*(8), 081801. https://doi.org/10.1115/1.4062175

Ferrari, A., Magnini, M., & Thome J. R. (2018). Numerical analysis of slug flow boiling in square microchannels. *International Journal of Heat and Mass Transfer*, *123*, 928-944. https://doi.org/10.1016/j.ijheatmasstransfer.2018.03.012

Gungor, K. E., & Winterton, R. H. (1986). A general correlation for flow boiling in tubes and annuli. *International Journal of Heat and Mass transfer*, *29*, 351-358. https://doi.org/10.1016/0017-9310(86)90205-X

Hassani, M., & Kouhikamali, R. (2020). Heat and mass modeling of R-245fa and R1233zd(E) with concurrent boiling and convective evaporation in falling film applications. *International Journal of Refrigeration*, *117*, 181-189. https://doi.org/10.1016/j.ijrefrig.2020.05.002

Hassani, M., Bagheri Motlagh, M., & Kouhikamali, R. (2020). Numerical investigation of upward air-water annular, slug and bubbly flow regimes. *Journal of Computational and Applied Research in Mechanical Engineering*, *9*(2), 331-341. https://10.22061/jcarme.2019.3893.1453

Hirt, C., & Nichols, B. (1981). Volume of fluid (VOF) method for the dynamics of free boundries. *Journal of Computational Physics*, *39*, 201-225. https://doi.org/10.1016/0021-9991(81)90145-5

Jaeger, J., Santos, C. M., Rosa, L. M., Meier, H. F., & Noriler, D. (2018). Experimental and numerical evolution of slugs in a vertical air-water flow. *Internatiol Journal of Multiphase Flow*, *101*, 152-166. https://doi.org/10.1016/j.ijmultiphaseflow.2018.01.009

Kouhikamali, R. (2010). Numerical simulation and parametric study of forced convective condensation in cylindrical vertical channels in multiple effect desalination systems. *Desalination*, *254*, 49–57. https://doi.org/10.1016/j.desal.2009.12.015

Krepper, E., & Rzehak, R. (2011). CFD for subcooled flow boiling: Simulation of DEBORA experiments. *Nuclear Engineering and Design*, *241*, 3851-3866. https://doi.org/10.1016/j.nucengdes.2011.07.003

Krepper, E., Koncar, B., & Egorov, Y. (2007). CFD modelling of subcooled boiling—concept, validation and application to fuel assembly design. *Nuclear Engineering and Design*, *237*, 716-731. https://doi.org/10.1016/j.nucengdes.2006.10.023

Lagus, T. P., & Kulacki, F. A. (2012). Two-phase heat transfer and bubble characteristics in a microchannel array. *Journal of Heat Transfer-Transactions of the ASME*, *134* (7). https://doi.org/10.1115/1.4006097

Lee, W. (1979). *A Pressure iteration scheme for two-phase modeling. Los Alamos Scientific Laboratory*. Los Alamos, New Mexico: Technical Report LA-UR, 79-975. https://doi.org/10.1142/9789814460286_0004

Li, H., Vasquez, S. A., Punekar, H., & Muralikrishnan, R. (2011*). Prediction of boiling and critical heat flux using an eulerian multiphase boiling model*. ASME, Denver, Colorado: International Mechanical Engineering Congress & Exposition, 463-476. https://doi.org/10.1115/IMECE2011-65539

Ling, T., Wang, T., Lei, G., Fang, Z., Zhao, L., & Xu, C. (2021). Experimental study on slug flow characteristics and its suppression by microbubbles in gas-liquid mixture pipeline. *Journal of Applied Fluid Mechanics*, *14*(2), 567-579. 10.47176/jafm.14.02.31482

Magnini, M., & Thome, J. R. (2016). Computational study of saturated flow boiling within a microchannel in the slug flow regime. *Journal of Heat Transfer-Transactions of the ASME*, *138* (2). https://doi.org/10.1115/1.4031234

Magnini, M., Pulvirenti, B., & Thome, J. R. (2013). Numerical investigation of influence of leading and sequential bubbles on slug flow boiling within a microchannel. *International Journal of Thermal Sciences*, *71*, 36-52. https://doi.org/10.1016/j.ijthermalsci.2013.04.018

Medina, C. D., Bassani, C. L., Cozin, C., Barbuto, F. A. A., Juqueira, S. L. M., & Morales, R. E. (2015). Numerical simulatio of the heat transfer in fully developed horizontal two-phase slug flows using a slug tracking method. *Internatioal Journal of Thermal Sciences*, *88*, 258-266. https://doi.org/10.1016/j.ijthermalsci.2014.05.007

Mehdipour, R., Baniamerian, Z., & Delauré, Y. (2016). Three dimensional simulation of nucleate boiling heat and mass transfer in cooling passages of internal combustion engines. *Heat Mass Transfer*, *52*, 957–968. https://doi.org/10.1007/s00231-015-1611-6

Mehdizadeh Momen, A., Sherif, S. A., & Lear, W. E. (2016). An analytical-numerical model for two-phase slug flow through a sudden area change in microchannels. *Journal of Applied Fluid Mechanics*, *9*(4), 1839-1850. 10.18869/acadpub.jafm.68.235.24576

Montenegro, G., D'Errico, G., Della Torre, A., Cadei, L., & Masi, S. (2016). Slug catcher multiphase CFD modeling: optimization and comparison with industrial standards. *Journal of Applied Fluid Mechanics*, *9*(1), 1-9. 10.36884/jafm.9.SI1.25816

Pan, Z., Weibel, J. A., & Garimella, S. V. (2016). A saturated-interface-volume phase change model for simulating flow boiling. *International Journal of Heat and Mass Transfer*, *93*, 945–956. https://doi.org/10.1016/j.ijheatmasstransfer.2015.10.044

Schmelter, S., Olbrich, M., Schmeyer, E., & Bär, M. (2020) Numerical simulation, validation, and analysis of two-phase slug flow in large horizontal pipes. *Flow Measurment and Instrumentation*, *73*, 101722. https://doi.org/10.1016/j.flowmeasinst.2020.101722

Shah, M. M. (1976). A new correlation for heat transfer during boiling flow through pipes. *ASHRAE Transactions*, *82*, 66-86.

Shah, M. M. (1982). Chart correlation for saturated boiling heat transfer: equations and further study. *Ashrae Trans*, *88*, 185-196.

Shih, T. H., Liou, W. W., Shabbir, A., Yang, Z., & Zhu, J. (1995). A new k-epsilon eddy viscosity model for high Reynolds number turbulent Flows - model development and validation. *Computers and Fluids*, *24*, 227–238. https://doi.org/10.1016/0045-7930(94)00032-T

Shin, H. C., Senguttuvan, S., & Kim, S. M. (2023). Experimental study on sub-regimes of air-water slug flow in a rectangular micro-channel. *International Journal of Mechanical Sciences*, *259*, 108577. https://doi.org/10.1016/j.ijmecsci.2023.108577

Simões, E. F., Carneiro, J. N. E., & Nieckele, A. O. (2014). Numerical prediction of non-boiling heat transfer in horizontal stratified and slug flow by the Two-Fluid Model. *International Journal of Heat and Fluid Flow*, *47*, 135-145. https://doi.org/10.1016/j.ijheatfluidflow.2014.03.005

Steiner, D., & Taborek, J. (1992). Flow boiling heat transfer in vertical tubes correlated by an asymptotic model. *Heat Transfer Engineering*, *13*, 43-69. https://doi.org/10.1080/01457639208939774

Sumith, B., Kaminaga, F., & Matsumura, K. (2003). Saturated flow boiling of water in a vertical small diameter tube. *Experimental Thermal and Fluid Science*, *27*, 789-801. https://doi.org/10.1016/S0894-1777(02)00317-5

Sun, D. L., Xu, J. L., & Wang, L. (2012). Development of a vapor–liquid phase change model for volume-of-fluid method in FLUENT. *International Communications in Heat and Mass Transfer*, *39*, 1101–1106. https://doi.org/10.1016/j.icheatmasstransfer.2012.07.020

Taha, T., & Cui, Z.F. (2006). CFD modelling of slug flow in vertical tubes. *Chemical Engineering Science*, *61*, 676-687. https://doi.org/10.1016/j.ces.2005.07.022

Wang, T., Gui, M., Zhang, T., Bi, Q., Zhao, J., & Liu, Z. (2021). Experimental investigation on characteristics parameters of air-water slug flow in a vertical tube. *Chemical Engineering Science*, *246*, 116895. https://doi.org/10.1016/j.ces.2021.116895

Yan, K., & Che, D. (2011). Hydrodynamic and mass transfer characteristics of slug flow in a vertical pipe with and without dispersed small bubbles. *International Journal of Multiphase Flow*, *37*, 299-325. https://doi.org/10.1016/j.ijmultiphaseflow.2010.11.001

Yang, Z., Peng, X., & Ye, P. (2008). Numerical and experimental investigation of two phase flow during boiling in a coiled tube. *International Journal of Heat and Mass Transfer*, *51*, 1003-1016. https://doi.org/10.1016/j.ijheatmasstransfer.2007.05.025